ACS Photonics

Article

pubs.acs.org/journal/apchd5

Mesoporous GaN for Photonic Engineering—Highly Reflective GaN Mirrors as an Example

Cheng Zhang,[†] Sung Hyun Park,[†] Danti Chen,[†] Da-Wei Lin,[‡] Wen Xiong,[§] Hao-Chung Kuo,[‡] Chia-Feng Lin,[∥] Hui Cao,[§] and Jung Han*[,†]

[†]Department of Electrical Engineering, Yale University, New Haven, Connecticut 06511, United States

[‡]Department of Photonics and Institute of Electro-Optical Engineering, National Chiao Tung University, Hsinchu 300, Taiwan

[§]Department of Applied Physics, Yale University, New Haven, Connecticut 06511, United States

[∥]Department of Materials Science and Engineering, National Chung Hsing University, Taichung 402, Taiwan

S *Supporting Information*

ABSTRACT: A porous medium is a special type of material where voids are created in a solid medium. The introduction of pores into a bulk solid can profoundly affect its physical properties and enable interesting mechanisms. In this paper, we report the use of mesoporous GaN to address a long-standing challenge in GaN devices: tuning the optical index in epitaxial structures without compromising the structural and electrical properties. By controlling the doping and electrochemical etching bias, we are able to control the pore morphology from macro- to meso- and microporous. The meso- and microporous GaN can be considered a new form of GaN with unprecedented optical index tunability. We examine the scattering loss in a porous medium quantitatively using numerical, semiempirical, and experimental methods. It is established that the optical loss due to scattering is well within the acceptable range. While being perfectly lattice-matched to GaN, the porous GaN layers are found to be electrically highly conductive. As an example of optical engineering, we demonstrate record high reflectances (R > 99.5%) from epitaxial mesoporous GaN mirrors that can be controllably fabricated, a result that is bound to impact GaN opto and photonic technologies.

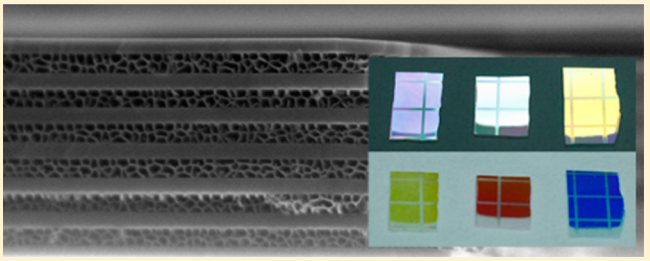

KEYWORDS: *mesoporous, photonic engineering, distributed Bragg reflector, electrochemical etching, gallium nitride, vertical-cavity surface-emitting laser*

A porous medium is a special type of material where voids/pores are created in an otherwise continuously solid medium. The term nanoporous (NP) media refers broadly to media having pore sizes of 100 nm or less. Depending on the characteristic length (d) of the pores, nanoporous media are further categorized into microporous (d < 2 nm), mesoporous (2 nm < d < 50 nm), and macroporous (d > 50 nm) classes. The introduction of pores into a bulk solid can profoundly affect its physical properties and enable interesting mechanisms. For instance, micro- and mesoporous media are widely used in catalysis and separation thanks to a greatly increased surface-to-volume ratio.[1] Porous silicon has attracted worldwide attention because of unexpected light emission from low-dimensional structures.[2] Recently we reported the preparation of NP-GaN using an electrochemical process.[3,4] After the porosification process, the NP-GaN maintains its single-crystallinity while acquiring many new characteristics.[5] Pores in macroporous GaN induce optical inhomogeneity such that visible-light propagation undergoes strong scattering, which is a very desirable attribute for enhancing the external quantum efficiency of light-emitting diodes (LEDs).[6,7] We also demonstrated that the elastic modulus of GaN can be reduced with an increase in porosity.[8] Having a large surface area, nanoporous GaN is energetically unstable against annealing (Rayleigh instability). Novel configurations and shapes of GaN can be obtained through curvature-driven mass transport at elevated temperatures.[9] NP-GaN can also be used in directing and blocking current flow after its conversion to resistive GaOx.[10] In this paper, we focus on the new possibility of using finely structured mesoporous GaN to control the index of refraction (n) of GaN, which is of crucial importance for optical engineering of GaN devices.

In conventional AlGaAs lasers and microcavities, optical mode confinement is achieved through epitaxy since the AlAs−GaAs system has a sufficiently large index contrast for the binary components (n = 2.89 and 3.42, respectively) and nearly perfect lattice matching. Parallel efforts in making AlGaN photonic devices encounter a major challenge as the AlN−GaN system has a severe lattice mismatch of 2.4%, unlike the nearly perfectly matched AlAs−GaAs system. Creating a modest contrast of only 0.2 in the AlGaN system would require

Received: April 25, 2015
Published: June 18, 2015

DOI: 10.1021/acsphotonics.5b00216
ACS Photonics 2015, 2, 980−986

extremely challenging epitaxy of $Al_{0.5}Ga_{0.5}N$ on GaN. The preparation of GaN microcavities using AlN/GaN distributed Bragg reflectors (DBRs) is one of the most challenging topics in III−nitride materials research after two decades of endeavors.[11−16] Even for commercial GaN blue laser diodes, the optical cladding structures represent a design trade-off that produces a relatively low optical confinement factor.[17] The purpose of this paper is to demonstrate the possibility and potential of using mesoporous GaN to provide unprecedented tunability in the index of refraction. Mesoporous GaN is especially remarkable in its homoepitaxial compatibility with GaN while maintaining a nearly lossless character from scattering and excellent electrical conductivity. As an example of optical engineering, we demonstrate record high reflectances (R > 99.5%) from epitaxial GaN DBRs[18] that can be controllably fabricated, a result that is bound to impact GaN opto and photonic technologies.

The recently discovered process of porosifying GaN electrochemically[3,4] will be briefly discussed here. When a positive anodic bias is applied to an n^+-type GaN sample immersed in an acid-based electrolyte, the n^+-GaN becomes oxidized by holes at the surface inversion layer. The surface oxide layer is subsequently dissolved in a suitable electrolyte.[19] With the use of electrochemical (EC) etching, one can either etch or porosify GaN according to specific process conditions.[4,19−21] In an EC etching experiment, the two most important parameters are the anodic bias and the conductivity of the layers. Without loss of generality, we show in Figure 1a

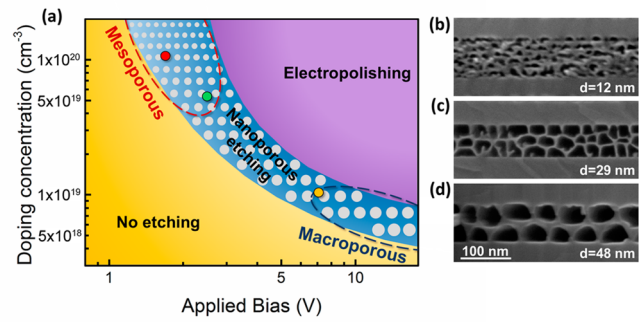

Figure 1. (a) Processing phase diagram for EC etching. The red dashed line encircles the mesoporous region for photonic applications, and the blue dashed line encompasses the macroporous region for light-scattering applications. (b−d) SEM images of NP-GaN etched according to the (b) red, green (c), and (d) yellow conditions in (a).

an etching phase diagram, which can be divided into three regions. When the applied bias or the doping concentration is low, no chemical reactions occur and GaN remains intact (yellow region). As the applied bias or the doping concentration increases, electrostatic breakdown occurs with the injection of holes into certain localized hot spots, resulting in the formation of porous structures through localized dissolution (blue region). At an even higher applied bias or with a higher doping concentration, electropolishing (complete etching) takes place (purple region).

Within the nanoporous region, the pore morphology can be controlled by the sample conductivity and the anodic bias. A higher doping level facilitates the formation of high-curvature mesopores,[4] and the threshold bias of porosification is reduced accordingly. Such tunability is illustrated in Figure 1b−d, where the doping concentration was varied from 1×10^{19} to 1×10^{20} cm^{-3}, corresponding to the red, green, and yellow dots in Figure 1a. The resulting NP-GaN can assume morphologies ranging from macroporous ($d \sim 50$ nm; Figure 1d) to mesoporous ($d \sim 30$ nm; Figure 1c) and approaching microporous ($d \sim 10$ nm; Figure 1b) in the upper left portion of the phase diagram.

Propagation of electromagnetic waves in a heterogeneous nonabsorbing medium consisting of small air voids has been analyzed.[22] It was established through numerical modeling that when the pore diameter (d) is much less than the wavelength, specifically when the scattering factor $\chi = \pi d/\lambda$ is less than 0.2, the index of refraction of a nanoporous medium can be described by the volume average theory (VAT), where $n_{eff} = [(1 - \varphi)n_{GaN}^2 + \varphi n_{air}^2]^{1/2}$, in which φ is the porosity.[22] For a photonic device operating in the blue or green wavelength regime, the mesopores or micropores will satisfy this criterion. NP-GaN therefore offers an elegant solution as a low-index medium to provide optical confinement to GaN while maintaining an aluminum-free, all-GaN structure that can be easily prepared (homo)epitaxially.

To demonstrate the practical utility of this mesoporous medium, we prepared a DBR made of GaN/mesoporous GaN. The history and challenges of making epitaxial GaN DBRs can be found in the Supporting Information and will not be repeated here. Figure 2a−c illustrates the process flow of making the mesoporous GaN DBR mirrors. First an epitaxial structure consisting of alternating n^+-GaN and GaN layers is grown (Figure 2a). Since the EC etching is designed in this case to proceed laterally, the sample needs to be lithographically patterned with trenches (via windows) to expose the side walls of the alternating layers (Figure 2b). The top of the sample surface is covered with SiO_2, while the edge (not shown) is connected to a source meter so the anodic bias can be applied. EC etching is then conducted wherein lateral porosification proceeds from the exposed side walls in the direction perpendicular to the side wall surface to form parallel nanopores (Figure 2c).

Figure 2d shows a top-view optical microscopy image of such a sample that has been patterned and laterally porosified. The dark-green patterns are vias/trenches created by inductively coupled plasma reactive-ion etching (ICP-RIE). Around these patterns mesoporous GaN is formed laterally, and these NP-GaN regions appear in light-green color under the optical microscope because of their greatly increased reflectance. The rate of lateral porosification is ∼5 μm/min. The area of the DBR region easily exceeds 50 μm, which is sufficiently large for the fabrication of vertical-cavity surface-emitting lasers (VCSELs). Figure 2e shows a cross-sectional scanning electron microscopy (SEM) image of a porous GaN DBR near the center of the cross-shaped alignment mark. A close-up SEM image of the same structure is shown in Figure 2f. The NP-GaN has a porosity of ∼70% and an average pore size of 30 nm. The DBR structure is formed by the conductivity-based selectivity in EC porosification, which cannot be accomplished by any other means, including photoassisted EC process.

The reflectance spectrum of the GaN/NP-GaN DBR was measured with a microreflectance setup calibrated against a commercial silver mirror with a spot size of 20 μm. The reflectance of sapphire was also measured and compared with published data, and it was determined that the accuracy is within 0.1%. The red solid line in Figure 3a shows the reflectance trace of a GaN/NP-GaN DBR sample with a stop band centered at ∼520 nm. The cross-sectional SEM image in

DOI: 10.1021/acsphotonics.5b00216
ACS Photonics 2015, 2, 980−986

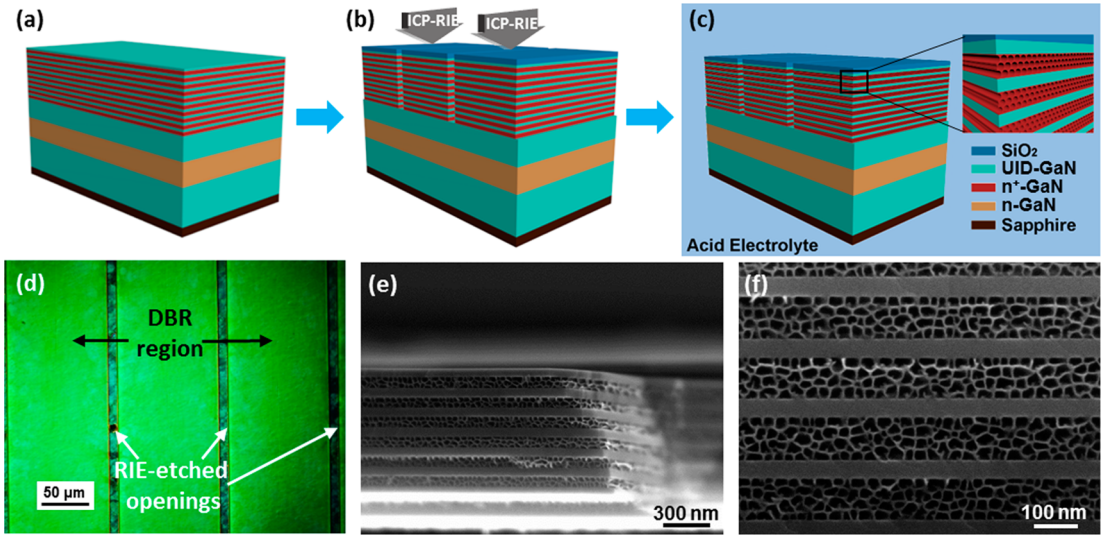

Figure 2. (a–c) Schematic process flow for the formation of a highly reflective DBR mirror with NP-GaN layers: (a) Epitaxial growth of $\lambda/4$ n^+-GaN/GaN structures. (b) Opening of via windows through dry etching to expose the side walls of n^+-GaN layers. (c) Electrochemical etching to convert n^+-GaN into NP-GaN laterally and selectively. The NP-GaN bears a morphology of parallel nanotubes (inset). (d) Top-view optical micrograph showing via openings (dark-green regions labeled by white arrows) and the highly reflective GaN/NP-GaN DBR regions (light-green regions labeled by black arrows). (e) Cross-sectional SEM image of a GaN/NP-GaN DBR structure. (f) Zoomed-in cross-sectional SEM image of a GaN/NP-GaN DBR structure.

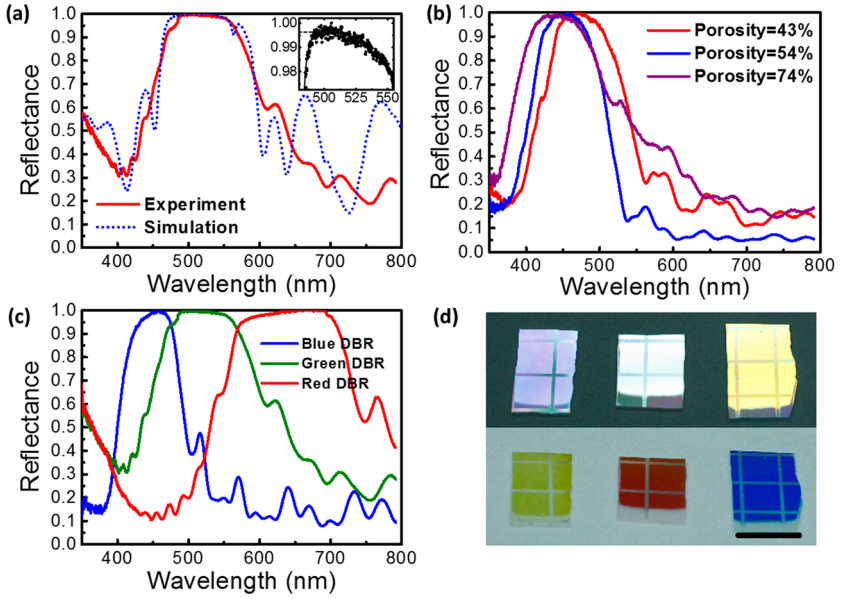

Figure 3. (a) Experimentally measured (red solid line) and COMSOL-simulated (blue dotted line) reflectance spectra from a DBR region. Inset: close-up of a reflectance spectrum (dots, experimental data; line, fit to the data) with a peak reflectance exceeding 99.5%. (b) Reflectance from three NP-GaN DBRs in the blue wavelength region obtain by tuning of the porosity. (c) Reflectance from three NP-GaN DBRs in the blue, green, and red wavelength regions. (d) Photographs of the three NP-GaN DBR mirrors in (c) under room-light illumination, showing process uniformity (scale bar = 1 cm). The top photograph was taken under incandescent light with continuous spectrum, the color of which reflects the DBRs' reflectance spectra, and the bottom photograph was taken under fluorescent light with distributed wavelengths, the color of which represents scattering of complementary wavelengths.

Figure 2f was scanned digitally as an input file for simulation, and the COMSOL-simulated reflectance is shown as the blue dotted line in Figure 3a. The difference between the simulation and the measured results is probably due to the relatively large numerical aperture (around 0.34) used in the reflectance measurement. Nevertheless, a peak reflectance of more than 99.5% is reproducibly obtained with a stop band of at least 70 nm (Figure 3a inset). We stress the fact that the peak reflectance reported here is among the highest reported from a III–nitride epitaxial DBR structure, and the full width at half-maximum (fwhm) is nearly 1 order of magnitude wider.[12−14]

To demonstrate the controllability of the mesoporous GaN DBRs, we systematically varied two parameters. First, we used the same as-grown structures but changed the anodic bias to change the porosity. Varying the porosity from 40 to 75% caused detuning by changing the index and the Bragg condition; the peak wavelength of the stop band can vary up to 30 nm for a blue GaN/NP-GaN DBR (Figure 3b).

DOI: 10.1021/acsphotonics.5b00216
ACS Photonics 2015, 2, 980–986

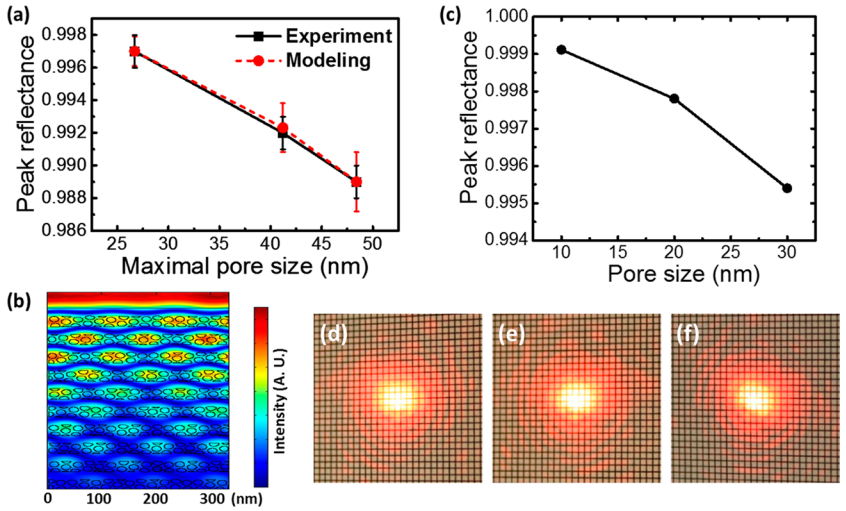

Figure 4. (a) Experimentally measured (black squares) and semiempirically modeled (red circles) peak reflectance vs maximum pore size at 450 nm. The error bar in the modeling comes from the error in the average pore size measurement, and the experimental error bar is based on the standard error from three consecutive reflectance measurements. (b) Electric field distribution in a GaN/NP-GaN DBR with a pore size of 30 nm. (c) COMSOL simulation of peak reflectance vs porosity. (d–f) Photographs of the far-field pattern: (d) red laser pointer 5 m from the screen; (e) the same laser reflected by an Al mirror 5 m away from the screen; (f) the same experiment with the Al mirror replaced by a NP-GaN DBR mirror (the grid is 1 mm).

Separately, we prepared three structures with different thicknesses but the same doping by metal–organic chemical vapor deposition. These acted as highly reflective (>99.5%) DBR mirrors in the blue (440 nm), green (520 nm), and red (600 nm) wavelength ranges (Figure 3c). Since no heteroepitaxy was involved, the preparation of these three structures was quite straightforward. The corresponding photographs of these mesoporous GaN DBR mirrors under room-light illumination are shown in Figure 3d.

While high reflectance has been demonstrated above, it seems counterintuitive that a porous medium can be used as a nearly perfect specular mirror. We therefore developed a semiempirical model regarding scattering. In the semiempirical analysis, we note that when the scattering factor $\chi = \pi d/\lambda$ is (much) less than 1, the scattering is analyzed by Rayleigh scattering.[23] A semiempirical equation for Rayleigh scattering was used to analyze the scattering loss:

$$\frac{I_{\mathrm{scatt}}}{I_0} = A\left(\frac{\pi d_{\mathrm{max}}}{\lambda}\right)^4 \frac{\varphi}{\pi {d_{\mathrm{avg}}}^2}$$

in which the factor $(\pi d_{\mathrm{max}}/\lambda)^4$ is the classic Rayleigh scattering dependence from a single scatterer, the factor $\varphi/\pi {d_{\mathrm{avg}}}^2$ (where φ is the porosity) gives the density of the scattering nanopores, and A is a fitting parameter. Since there is a finite size dispersion in the nanopores, we used the maximum pore diameter estimated from SEM, d_{max}, in the calculation of the scattering factor (χ). In Figure 4a, the experimentally measured peak reflectance at λ = 450 nm (black squares) is correlated with the semiempirical Rayleigh model (red circles) for several samples with varying pore sizes. The good agreement indicates that the detected scattering is indeed of the Rayleigh kind.

Going further beyond the semiempirical treatment of Rayleigh scattering, we employed a finite-element solver (COMSOL Multiphysics 5.0 RF Module) to model numerically the propagation and scattering of an electromagnetic (EM) wave in a mesoporous GaN DBR structure. A digitized image of GaN/NP-GaN DBR was constructed assuming a two-dimensional axisymmetric distribution of straight parallel nanopores, which was a good approximation to the actual pore morphology as illustrated in the Figure 2c inset. An example of the simulated electric field distribution for a propagating EM wave is shown in Figure 4b. The irregular solid shapes (with an average pore size of 30 nm) denote pores that are spaced between GaN layers. The false-color plot shows the exponential decay of EM waves into the DBR structure, and the peaks of the EM field coincide with the center of the low-index porous layer. The lateral periodic modulation in the EM field intensity is likely an artifact in numerical modeling because we used the digitized image as a unit cell to generate the full DBR structure. The simulated peak reflectance as a function of the pore size is plotted in Figure 4c. One should note the very good agreement between Figure 4a (semiempirical and experimental data) and Figure 4c (numerical data). The numerical modeling provided additional proof that DBRs with very high reflectance can be constructed from carefully prepared mesoporous GaN.

To determine the potential impact of GaN/NP-GaN DBR mirrors on the wavefront (or phase coherence), we examined the far-field pattern of a diode laser before and after reflection by the mesoporous mirror at a 45° angle of incidence. We used a red laser pointer (λ = 652 nm) with an intrinsic beam divergence of around 0.1°, causing a broadening of the spot size of ~8 mm over a distance of 5 m (Figure 4d). To study the effect of reflection, we used a reference Al mirror (having a reflectivity similar to that of the red DBR at 652 nm) side by side with the mesoporous GaN mirror under testing. Comparison of the two reflected images (Figure 4e,f) indicated that neither mirror produces any appreciable amount of divergence in the far-field pattern. The broadening of the lasing wavefront (Gaussian beam width), if any, should be much less than the original beam divergence of 0.1°. The speckle patterns around the laser spot that indicate phase coherence are also preserved. The study above, combining semiempirical, numerical, and experimental investigations, affirms that mesoporous GaN DBRs will be a legitimate and unique building block for III–nitride opto and photonic devices.

DOI: 10.1021/acsphotonics.5b00216
ACS Photonics 2015, 2, 980–986

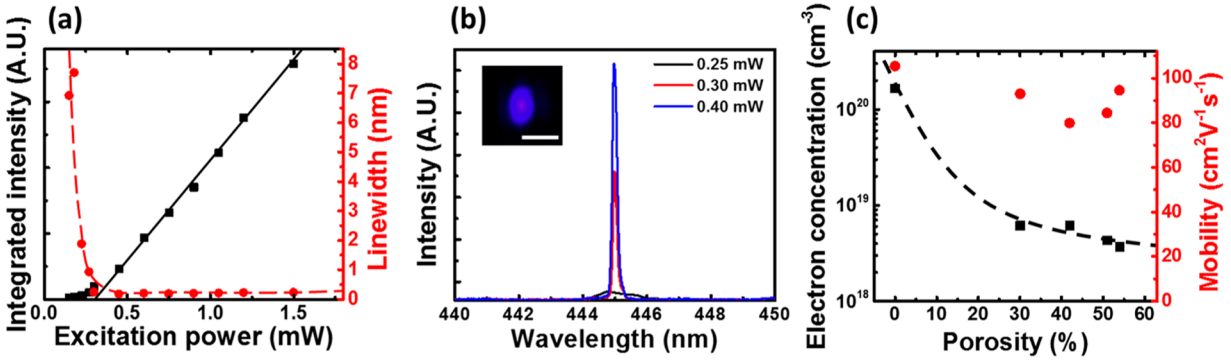

Figure 5. (a) Laser output intensity and line width as functions of the excitation power. (b) Output spectra at different excitation powers (below, at, and above threshold) originating from an optically pumped microcavity with a GaN/NP-GaN bottom DBR and a dielectric top DBR. Single-mode lasing at 445 nm with a line width of 0.17 nm was achieved above threshold. Inset: far-field laser spot from optical pumping of the microcavity (scale bar = 5 mm). (c) Analysis of electron concentration and mobility with respect to porosity in mesoporous GaN.

A planar InGaN microcavity was constructed using the mesoporous GaN structure described above as the bottom DBR mirror. The microcavity for optical pumping was completed with 10 $In_{0.15}Ga_{0.85}N$ (3 nm)/GaN (8 nm) quantum wells (λ_{PL} = 450 nm) capped with 12 pairs of dielectric SiO_2/TiO_2 layers as the top mirror. The cavity was designed to have an overall effective length of 3λ, and the InGaN multiple quantum wells (MQWs) were placed at an antinode. Optical pumping was performed with a 355 nm pulsed laser (pulse duration of 0.5 ns and pulse rate of 1 kHz). Figure 5a shows the output intensity and line width as functions of the excitation power. A clear lasing threshold can be observed at a power density of 1.5 kW/cm^2. Figure 5b shows the output spectra at different excitation powers (below, at, and above threshold). Single-mode lasing was achieved at 445 nm with a line width of 0.17 nm. In this preliminary design where the cavity resonance is yet to match precisely with the MQWs peak emission, we measured a lasing quality (Q) factor of more than 3000 and a below-threshold (cold cavity) Q factor of around 500. The presence of surface-emitting laser action was further established from a far-field (40 cm away) spot pattern (Figure 5b inset) showing a nearly circular beam profile. Finally, as a step toward a current-injection DBR structure for GaN VCSELs, we studied the transport property of porous GaN using Hall measurements. An n^+-GaN layer ($n > 1 \times 10^{20}$ cm^{-3}) was porosified, and the measured concentration and mobility were plotted versus the porosity (Figure 5c). While the effective carrier concentration is reduced as the porosity increases, the overall carrier concentration still exceeds 1×10^{18} cm^{-3} for a porosity of up to 55%, and the mobility remains nearly constant at 100 cm^2 V^{-1} s^{-1}.

To summarize, we have developed an electrochemical method to form high-reflectivity (R > 99.5%) conductive mesoporous GaN DBRs. The properties of this new mesoporous GaN are summarized in Figure 6, together with those of other layers used for III−V and III−nitride photonics for comparison. AlAs−GaAs and InP−AlInAs−GaInAs systems have enabled many long-wavelength photonic devices as a result of their good index contrasts (Δn), nearly zero mismatched stresses, and very low resistivities, thus having a good vertical span while staying close to the z axis. The candidates for III−nitride photonic engineering prior to our work include AlGaN and SiO_2/TiO_2. The former system is highly slanted in Figure 6, indicating that a modest change in refractive index causes great tensile stress and a great increase in resistivity. The dielectric system has large index constrasts and low stress but is insulating. Using mesoporous GaN introduces a new tunability with a vertical span exceeding those of the III−V materials while remaining stress-free with low resistivity. This method is promising to solve the long-standing challenges in realizing high-performance VCSELs and edge-emitting laser diodes.

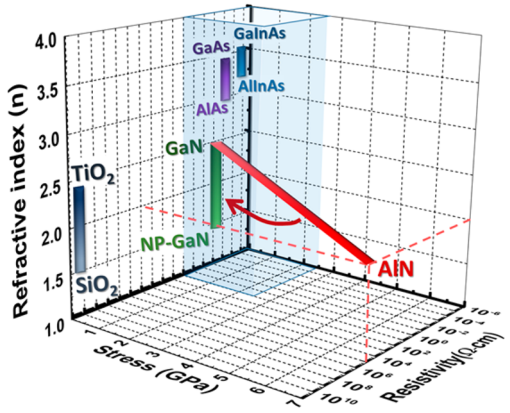

Figure 6. Three-dimensional parameter plot for NP-GaN in comparison with other photonic materials.[24−39] The NP-GaN system introduces a new material tunability in photonic engineering among high-quality and electrically desirable materials systems, as signified in the light-blue region.

■ ASSOCIATED CONTENT

Supporting Information

Experimental section and a table of AlGaN-based DBR properties compiled from the literature. The Supporting Information is available free of charge on the ACS Publications website at DOI: 10.1021/acsphotonics.5b00216.

■ AUTHOR INFORMATION

Corresponding Author

*E-mail: jung.han@yale.edu.

Notes

The authors declare no competing financial interest.

■ ACKNOWLEDGMENTS

This research was supported by the National Science Foundation (NSF) under Award CMMI-1129964, and facilities used were supported by YINQE and NSF MRSEC DMR

DOI: 10.1021/acsphotonics.5b00216
ACS Photonics 2015, 2, 980−986

1119826. We acknowledge Prof. Arto Nurmikko's group (Kwangdong Roh) from Brown University for their kind help with reflectance measurements on mesoporous GaN DBRs.

REFERENCES

(1) Davis, M. E. Ordered porous materials for emerging applications. *Nature* **2002**, *417*, 813−821.
(2) Cullis, A. G.; Canham, L. T.; Calcott, P. D. J. The structural and luminescence properties of porous silicon. *J. Appl. Phys.* **1997**, *82*, 909−965.
(3) Zhang, Y.; Ryu, S.-W.; Yerino, C.; Leung, B.; Sun, Q.; Song, Q.; Cao, H.; Han, J. A conductivity-based selective etching for next generation GaN devices. *Phys. Status Solidi B* **2010**, *247*, 1713−1716.
(4) Chen, D.; Xiao, H.; Han, J. Nanopores in GaN by electrochemical anodization in hydrofluoric acid: Formation and mechanism. *J. Appl. Phys.* **2012**, *112*, No. 064303.
(5) Mynbaeva, M.; Titkov, A.; Kryzhanovski, A.; Kotousova, I.; Zubrilov, A. S.; Ratnikov, V. V.; Davydov, V. Y.; Kuznetsov, N. I.; Mynbaev, K.; Tsvetkov, D. V.; Stepanov, S.; Cherenkov, A.; Dmitriev, V. A. Strain relaxation in GaN layers grown on porous GaN sublayers. *MRS Internet J. Nitride Semicond. Res.* **1999**, *4*, No. e14.
(6) Yang, C. C.; Lin, C. F.; Lin, C. M.; Chang, C. C.; Chen, K. T.; Chien, J. F.; Chang, C. Y. Improving light output power of InGaN-based light emitting diodes with pattern-nanoporous p-type GaN:Mg surfaces. *Appl. Phys. Lett.* **2008**, *93*, No. 203103.
(7) Lee, K. J.; Kim, S.-J.; Kim, J.-J.; Hwang, K.; Kim, S.-T.; Park, S.-J. Enhanced performance of InGaN/GaN multiple-quantum-well light-emitting diodes grown on nanoporous GaN layers. *Opt. Express* **2014**, *22*, A1164−A1173.
(8) Huang, S.; Zhang, Y.; Leung, B.; Yuan, G.; Wang, G.; Jiang, H.; Fan, Y.; Sun, Q.; Wang, J.; Xu, K.; Han, J. Mechanical Properties of Nanoporous GaN and Its Application for Separation and Transfer of GaN Thin Films. *ACS Appl. Mater. Interfaces* **2013**, *5*, 11074−11079.
(9) Yerino, C. D.; Zhang, Y.; Leung, B.; Lee, M. L.; Hsu, T.-C.; Wang, C.-K.; Peng, W.-C.; Han, J. Shape transformation of nanoporous GaN by annealing: From buried cavities to nano-membranes. *Appl. Phys. Lett.* **2011**, *98*, No. 251910.
(10) Lin, C.-F.; Lee, W.-C.; Shieh, B.-C.; Chen, D.; Wang, D.; Han, J. Fabrication of Current Confinement Aperture Structure by Transforming a Conductive GaN:Si Epitaxial Layer into an Insulating GaOx Layer. *ACS Appl. Mater. Interfaces* **2014**, *6*, 22235−22242.
(11) Redwing, J. M.; Loeber, D. A. S.; Anderson, N. G.; Tischler, M. A.; Flynn, J. S. An optically pumped GaN−AlGaN vertical cavity surface emitting laser. *Appl. Phys. Lett.* **1996**, *69*, 1−3.
(12) Waldrip, K. E.; Han, J.; Figiel, J. J.; Zhou, H.; Makarona, E.; Nurmikko, A. V. Stress engineering during metalorganic chemical vapor deposition of AlGaN/GaN distributed Bragg reflectors. *Appl. Phys. Lett.* **2001**, *78*, 3205−3207.
(13) Butté, R.; Feltin, E.; Dorsaz, J.; Christmann, G.; Carlin, J. F.; Grandjean, N.; Ilegems, M. Recent Progress in the Growth of Highly Reflective Nitride-Based Distributed Bragg Reflectors and Their Use in Microcavities. *Jpn. J. Appl. Phys.* **2005**, *44*, 7207−7216.
(14) Huang, G. S.; Lu, T. C.; Yao, H. H.; Kuo, H. C.; Wang, S. C.; Lin, C.-W.; Chang, L. Crack-free GaN/AlN distributed Bragg reflectors incorporated with GaN/AlN superlattices grown by metalorganic chemical vapor deposition. *Appl. Phys. Lett.* **2006**, *88*, No. 061904.
(15) Li, Z.-Y.; Lu, T.-C.; Kuo, H.-C.; Wang, S.-C.; Lo, M.-H.; Lau, K. M. HRTEM investigation of high-reflectance AlN/GaN distributed Bragg-reflectors by inserting AlN/GaN superlattice. *J. Cryst. Growth* **2009**, *311*, 3089−3092.
(16) Cosendey, G.; Castiglia, A.; Rossbach, G.; Carlin, J.-F.; Grandjean, N. Blue monolithic AlInN-based vertical cavity surface emitting laser diode on free-standing GaN substrate. *Appl. Phys. Lett.* **2012**, *101*, No. 151113.
(17) Han, J.; Li, Y. A method to make III−nitride edge emitting laser diode of high confinement factor with lattice matched cladding layer. Disclosure OCR 6697, 2015.
(18) During the preparation and submission of this article, we became aware of similar work focusing on macroscopic porous GaN structure. See: Lee, S.-M.; Gong, S.-H.; Kang, J.-H.; Ebaid, M.; Ryu, S.-W.; Cho, Y.-H. Optically pumped GaN vertical cavity surface emitting laser with high index-contrast nanoporous distributed Bragg reflector. *Opt. Express* **2015**, *23*, 11023−11030.
(19) Schwab, M. J.; Chen, D.; Han, J.; Pfefferle, L. D. Aligned Mesopore Arrays in GaN by Anodic Etching and Photoelectrochemical Surface Etching. *J. Phys. Chem. C* **2013**, *117*, 16890−16895.
(20) Park, J.; Song, K. M.; Jeon, S.-R.; Baek, J. H.; Ryu, S.-W. Doping selective lateral electrochemical etching of GaN for chemical lift-off. *Appl. Phys. Lett.* **2009**, *94*, No. 221907.
(21) Park, S. H.; Yuan, G.; Chen, D.; Xiong, K.; Song, J.; Leung, B.; Han, J. Wide Bandgap III−Nitride Nanomembranes for Optoelectronic Applications. *Nano Lett.* **2014**, *14*, 4293−4298.
(22) Braun, M. M.; Pilon, L. Effective optical properties of non-absorbing nanoporous thin films. *Thin Solid Films* **2006**, *496*, 505−514.
(23) Kerker, M. Rayleigh−Debye Scattering. In *The Scattering of Light and Other Electromagnetic Radiation*; Physical Chemistry: A Series of Monographs, Vol. *16*; Academic Press: New York, 1969; Chapter 8, pp 414−486.
(24) Theeten, J. B.; Aspnes, D. E.; Chang, R. P. H. A new resonant ellipsometric technique for characterizing the interface between GaAs and its plasma-grown oxide. *J. Appl. Phys.* **1978**, *49*, 6097−6102.
(25) Fern, R. E.; Onton, A. Refractive Index of AlAs. *J. Appl. Phys.* **1971**, *42*, 3499−3500.
(26) Indium phosphide (InP), electrical and thermal conductivity, carrier concentrations. In *Group IV Elements, IV−IV and III−V Compounds. Part b—Electronic, Transport, Optical and Other Properties*; Madelung, O., Rössler, U., Schulz, M., Eds.; Landolt-Börnstein—Group III Condensed Matter, Vol. *41A1b*; Springer: Berlin, 2002; pp 1−11.
(27) Mondry, M. J.; Babic, D. I.; Bowers, J. E.; Coldren, L. A. Refractive indexes of (Al,Ga,In)As epilayers on InP for optoelectronic applications. *IEEE Photonics Technol. Lett.* **1992**, *4*, 627−630.
(28) Schmidt, N. M. Indium Phosphide (InP). *Handb. Ser. Semicond. Parameters* **1997**, 169−190.
(29) Dias, I. F. L.; Nabet, B.; Kohl, A.; Benchimol, J. L.; Harmand, J. C. Electrical and optical characteristics of n-type-doped distributed Bragg mirrors on InP. *IEEE Photonics Technol. Lett.* **1998**, *10*, 763−765.
(30) King, P. D. C.; Veal, T. D.; McConville, C. F. Unintentional conductivity of indium nitride: Transport modelling and microscopic origins. *J. Phys.: Condens. Matter* **2009**, *21*, No. 174201.
(31) Barker, A. S.; Ilegems, M. Infrared Lattice Vibrations and Free-Electron Dispersion in GaN. *Phys. Rev. B* **1973**, *7*, 743−750.
(32) Crouch, R. K.; Debnam, W. J.; Fripp, A. L. Properties of GaN grown on sapphire substrates. *J. Mater. Sci.* **1978**, *13*, 2358−2364.
(33) Pastrňák, J.; Roskovcová, L. Refraction Index Measurements on AlN Single Crystals. *Phys. Status Solidi B* **1966**, *14*, K5−K8.
(34) Edwards, J.; Kawabe, K.; Stevens, G.; Tredgold, R. H. Space charge conduction and electrical behaviour of aluminium nitride single crystals. *Solid State Commun.* **1965**, *3*, 99−100.
(35) Gerlich, D.; Dole, S. L.; Slack, G. A. Elastic properties of aluminum nitride. *J. Phys. Chem. Solids* **1986**, *47*, 437−441.
(36) Gao, L.; Lemarchand, F.; Lequime, M. Refractive index determination of SiO_2 layer in the UV/vis/NIR range: spectrophotometric reverse engineering on single and bi-layer designs. *J. Eur. Opt. Soc.: Rapid Publ.* **2013**, *8*, No. 13010.
(37) Shackelford, J. F.; Alexander, W. *CRC Materials Science and Engineering Handbook*, 3rd ed.; CRC Press: Boca Raton, FL, 2000.
(38) Kischkat, J.; Peters, S.; Gruska, B.; Semtsiv, M.; Chashnikova, M.; Klinkmüller, M.; Fedosenko, O.; Machulik, S.; Aleksandrova, A.; Monastyrskyi, G.; Flores, Y.; Masselink, W. T. Mid-infrared optical properties of thin films of aluminum oxide, titanium dioxide, silicon dioxide, aluminum nitride, and silicon nitride. *Appl. Opt.* **2012**, *51*, 6789−6798.

DOI: 10.1021/acsphotonics.5b00216
ACS Photonics 2015, 2, 980−986

(39) Sarah, M. S. P.; Musa, M. Z.; Asiah, M. N.; Rusop, M. Electrical conductivity characteristics of TiO_2 thin film. In *Proceedings of the 2010 International Conference on Electronic Devices, Systems & Applications*; IEEE: New York, 2010; pp 361−364.

DOI: 10.1021/acsphotonics.5b00216
ACS Photonics 2015, 2, 980−986